Journal of Biomolecular NMR **27:** 365–375, 2003.
KLUWER/ESCOM

Cross correlations between ^{13}C-^{1}H dipolar interactions and ^{15}N chemical shift anisotropy in nucleic acids

Sapna Ravindranathan[a], Chul-Hyun Kim[b] & Geoffrey Bodenhausen[a,c,*]
[a]*Institut de Chimie Moléculaire et Biologique, Ecole Polytechnique Fédérale de Lausanne, BCH, 1015 Lausanne, Switzerland;* [b]*Department of Chemistry, University of California, Berkeley, CA 94720-1460, U.S.A.;* [c]*Département de Chimie, associé au CNRS, Ecole Normale Supérieure, 24, rue Lhomond, 75231 Paris Cedex 05, France*

Received 2 May 2003; Accepted 30 June 2003

Key words: anisotropic diffusion, chemical shift anisotropy, cross-correlation, glycosidic linkage, NMR, nucleic acid dynamics

Abstract

Two sets of cross-correlated relaxation rates involving chemical shift anisotropy and dipolar interactions have been measured in an RNA kissing complex. In one case, both the CSA and dipolar interaction tensors are located on the same nucleotide base and are rigidly fixed with respect to each other. In the other case, the CSA tensor is located on the nucleotide base whereas the dipolar interaction is located on the adjoining ribose unit. Analysis of the measured rates in terms of isotropic or anisotropic rotational diffusion has been carried out for both cases. A marked difference between the two models is observed for the cross-correlation rates involving rigidly fixed spin interactions. The influence of internal motions about the glycosidic linkage between the nucleotide base and the ribose unit on cross-correlated relaxation rates has been estimated by applying a model of restricted rotational diffusion. Local motions seem to have a more pronounced effect on cross-correlated relaxation rates when the two spin interactions are not rigidly fixed with respect to each other.

Introduction

Conformational dynamics play a significant role in determining the properties and biological functions of biomacromolecules. In nucleic acids various local motions can occur within the different moeities that make up the structure. For example, one must distinguish motions along the sugar-phosphate backbone, twist, tilt or roll motions of the nucleotide base planes, motions about the glycosidic base-sugar linkage and conformational dynamics within the sugar rings. Molecular motions can be assessed experimentally by analyzing NMR spin relaxation rates (Palmer et al., 1996; Palmer, 1997). The most common approach is to measure autocorrelated longitudinal relaxation rates (T_1), transverse relaxation rates (T_2) and heteronuclear Overhauser effects (NOE's) of ^{15}N or ^{13}C nuclei. These rates are proportional to spectral density functions which depend on the overall and local dynamics of the macromolecule. For macromolecules which have shapes that are approximately spherical, the overall tumbling motion can be described in terms of isotropic rotational diffusion characterized by a single correlation time τ_c^{iso}. Local motions can be interpreted according to the Lipari-Szabo formalism, in which the mobility in different parts of the macromolecule is expressed in terms of order parameters (Lipari and Szabo, 1982). For nucleic acid molecules however, the overall motion is often anisotropic and the interpretation of local motions in terms of order parameters is not as straightforward as in the case of molecules with isotropic overall motion. Complex models which describe anisotropic motions require additional parameters to represent dynamics. It is therefore of interest to design new experiments that provide additional observables for analysing anisotropic motions, both global and local.

*To whom correspondence should be addressed. E-mail: Geoffrey.Bodenhausen@ens.fr

The set of experimental observables can be expanded considerably by measuring cross-correlated relaxation rates. Cross-correlated relaxation arises from the interference of relaxation mechanisms involving two different spin interactions such as chemical shift anisotropy (CSA) and dipole-dipole (DD) interactions. Since cross-correlation rates depend on the relative orientations of pairs of spin interactions, they are sensitive to correlated motions of the spin interaction tensors due to internal conformational reorientations. We present here new experimental schemes which measure two cross-correlated relaxation rates, both of which involve the CSA of a ^{15}N spin and a ^{13}C-^{1}H dipolar interaction. The experiments have been carried out on an RNA kissing complex with the nucleotide sequence shown in Figure 1. The relevant CSA and DD interactions are indicated by ellipses in the figure. In Experiment A, we measure the cross-correlated relaxation rate involving the CSA of the glycosidic ^{15}N (N1 in pyrimidines and N9 in purines) and the ^{13}C-^{1}H dipolar interaction within the same nucleotide base (C6-H6 in pyrimidines and C8-H8 in purines). In this case, both spin interaction tensors are located within the same base and are rigidly fixed with respect to each other. In Experiment B, we measure the cross-correlated relaxation rate between the CSA of the same glycosidic ^{15}N and a ^{13}C-^{1}H dipolar interaction within the attached ribose ring (C1′-H1′). Here, the spin interactions are located on different structural moeities, namely on the nucleotide base and on the ribose unit. Thus the two interaction pairs are not rigidly fixed with respect to each other. We compare the measured rates with predictions for different models of global motion, namely isotropic tumbling and anisotropic tumbling with a cylindrical diffusion tensor. The effects of internal motions have been examined by applying the restricted rotational diffusion model to describe the flexibility about the glycosidic linkage between the nucleotide base and the ribose unit.

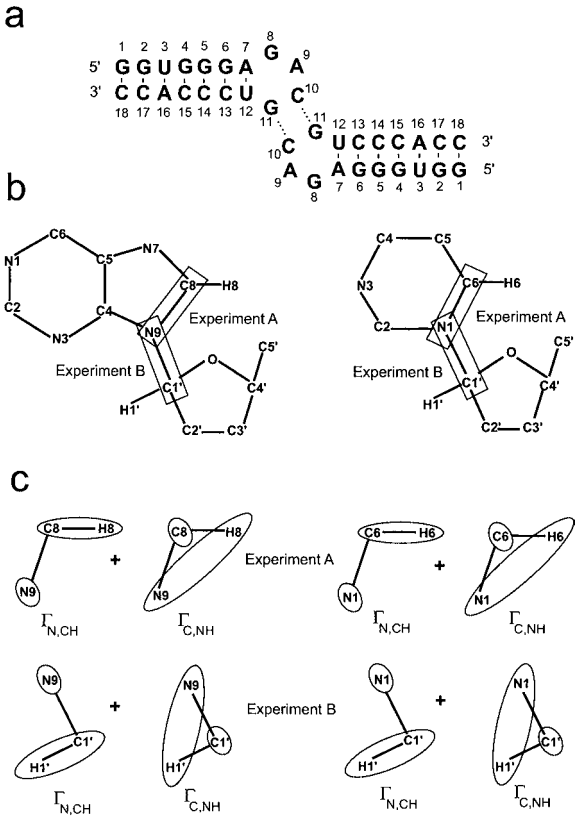

Figure 1. (a) Schematic nucleotide sequence of the RNA kissing complex. The intermolecular Watson–Crick base pairing C10-G11 leading to dimer formation is indicated by dotted lines. (b) Purine and pyrimidine nucleotide framework showing nuclei in rectangular frames between which double- and zero-quantum coherences are excited in Experiments A and B. (c) CSA and dipolar interactions giving rise to the cross-correlation rates measured in Experiments A and B.

Theoretical background

The experiments focus on an HCN spin system comprising the glycosidic ^{15}N spin and ^{13}C and ^{1}H spins belonging either to the nucleotide base or to the ribose unit. The double- and zero-quantum coherences involving the ^{13}C and ^{15}N spins have doublet components which resonate at $\omega_N + \omega_C \pm \pi(^1J_{CH} + ^2J_{NH})$ and $\omega_N - \omega_C \pm \pi(^1J_{CH} - ^2J_{NH})$, respectively. The doublet components of the double- and zero-quantum spectra relax at different rates under the influence of various cross-correlation effects due to the chemical shift anisotropy (CSA) and dipole-dipole (DD) interactions (Kumar et al., 2000). The relaxation rates of the double- and zero- quantum components are given by

$$\Gamma_{D\alpha} = \Gamma_a + \Gamma_{N,CH} + \Gamma_{C,NH} + \Gamma_{CH,NH} + \Gamma_{C,N} + \Gamma_{C,CH} + \Gamma_{N,NH}, \quad (1)$$

$$\Gamma_{D\beta} = \Gamma_a - \Gamma_{N,CH} - \Gamma_{C,NH} + \Gamma_{CH,NH} + \Gamma_{C,N} - \Gamma_{C,CH} - \Gamma_{N,NH}, \quad (2)$$

$$\Gamma_{Z\alpha} = \Gamma_a - \Gamma_{N,CH} - \Gamma_{C,NH} - \Gamma_{CH,NH} - \Gamma_{C,N} + \Gamma_{C,CH} + \Gamma_{N,NH}, \quad (3)$$

$$\Gamma_{Z\beta} = \Gamma_a + \Gamma_{N,CH} + \Gamma_{C,NH} - \Gamma_{CH,NH} - \Gamma_{C,N} - \Gamma_{C,CH} - \Gamma_{N,NH}, \quad (4)$$

where Γ_a is the autocorrelated relaxation rate and the terms $\Gamma_{i,jk}$, $\Gamma_{ik,jk}$, and $\Gamma_{i,j}$ refer to the cross-correlated relaxation rates involving CSA/DD, DD/DD and CSA/CSA interactions respectively. In experimental schemes which allow for the evolution of the double- and zero-quantum components over a constant time period, the differences in relaxation rates translate into differences in signal intensities of the doublet components in the double- and zero-quantum spectra (Reif et al., 1997; Schwalbe et al., 2001). Various cross-correlated relaxation rates can then be determined by taking appropriate intensity ratios of the double- and zero-quantum multiplet components observed in constant time experiments. This approach has been applied to measure cross-correlated relaxation rates associated with three-spin systems in proteins and nucleic acids (Brutscher et al., 1997; Yang et al., 1997; Richter et al., 2000).

Recently several experimental schemes have been introduced which incorporate π pulses in the relaxation interval to single out specific cross-correlation pathways (Felli et al., 1999; Chiarparin et al., 1999; Brutscher, 2000). An initial density operator term transforms under the selected cross-correlation pathway into a final density operator term and the cross-correlation rate is obtained by measuring signals proportional to the initial and final operator terms. In experiments involving relaxation of double- and zero-quantum coherences in an HCN spin system, these schemes permit the separation of the following combinations of cross-correlation rates; $\Gamma_{N,CH} + \Gamma_{C,NH}$; $\Gamma_{C,CH} + \Gamma_{N,NH}$ and $\Gamma_{CH,NH} + \Gamma_{C,N}$. Similar schemes can be introduced in constant time experiments for selecting the effects of specific cross-correlation pathways on double- and zero-quantum multiplets. This has been demonstrated in proteins for determining $C'/C^{\alpha}H^{\alpha}$ cross-correlation rates (Yang et al., 1998). We adopt a similar scheme to determine the $\Gamma_{N,CH} + \Gamma_{C,NH}$ cross-correlation rates in RNA.

In the pulse sequence shown in Figure 2, the π pulses applied during the constant time period T select the 'remote' CSA/DD cross-correlation terms, $\Gamma_{N,CH} + \Gamma_{C,NH}$ (Figure 1c). The effects of the 'local' CSA/DD cross-correlation terms, $\Gamma_{C,CH} + \Gamma_{N,NH}$, along with DD/DD and CSA/CSA cross- correlation terms such as $\Gamma_{CH,NH} + \Gamma_{C,N}$ are cancelled. The two 'remote' terms $\Gamma_{N,CH}$ and $\Gamma_{C,NH}$ are influenced in a similar fashion by the π pulses and hence cannot be separated. However, in favourable cases one of the terms (e.g., $\Gamma_{N,CH}$) will be dominant and the contribution of the other term (e.g., $\Gamma_{C,NH}$) can be neglected. In this experiment, the π pulses simplify the HCN spin system so that it behaves in effect like an NH spin system during the period T. The coherences present at the beginning of T evolve under the nitrogen chemical shift Ω_N and the scalar couplings ^{1}J(CH), resulting in a doublet centered at Ω_N. The relaxation rates of the doublet components are given by

$$\Gamma_{D\beta,Z\alpha} = \Gamma_a - (\Gamma_{N,CH} + \Gamma_{C,NH}), \quad (5)$$

$$\Gamma_{D\alpha,Z\beta} = \Gamma_a + (\Gamma_{N,CH} + \Gamma_{C,NH}). \quad (6)$$

The rate $\Gamma_{D\beta,Z\alpha}$ is the average of the rates $\Gamma_{D\beta}$ and $\Gamma_{Z\alpha}$ given in Equations 2 and 3, whereas the rate $\Gamma_{D\alpha,Z\beta}$ is the average of the rates $\Gamma_{D\alpha}$ and $\Gamma_{Z\beta}$ given by Equations 1 and 4. Under the influence of the π pulses the relaxation behaviour becomes analogous to that of an NH spin system in which the relaxation rates of the doublet components of N differ by the cross-correlation rate involving the CSA of spin N and the dipolar interaction between spins N and H. In our case however the dipolar interaction is between spins C and H. The cross-correlation rate can be measured from the intensity ratio of the doublet components

$$\Gamma_{N,CH} + \Gamma_{C,NH} = \frac{1}{2T} \ln\left(\frac{I_{D\beta,Z\alpha}}{I_{D\alpha,Z\beta}}\right). \quad (7)$$

This scheme has the advantage that the desired rate is obtained from the ratio of only two components instead of four which would be obtained in a constant time evolution experiment that does not employ any selection scheme. This leads to an improvement in sensitivity.

Assuming that the molecule undergoes isotropic overall motion and has no internal motions, the cross-correlation rate involving the CSA of spin i and a dipolar interaction between spins j and k is given by (Richter et al., 2000)

$$\Gamma^{iso}_{i,jk} = \frac{2}{3}\left(\frac{\mu_0\hbar}{4\pi}\right)\frac{\gamma_j\gamma_k}{r^3_{jk}}\gamma_i B_0 \times \sum_{n=1}^{2}(\sigma_i^{nn} - \sigma_i^{33}) P_2(\cos\Theta_{nn,jk}) \sum_q J(\omega_q), \quad (8)$$

$$J(\omega_q) = \frac{2}{5}\left(\frac{\tau_c^{iso}}{1 + (\omega_q\tau_c^{iso})^2}\right). \quad (9)$$

Here, B_0 is the magnetic field strength and γ_i, γ_j, γ_k are the gyromagnetic ratios of the spins i, j,

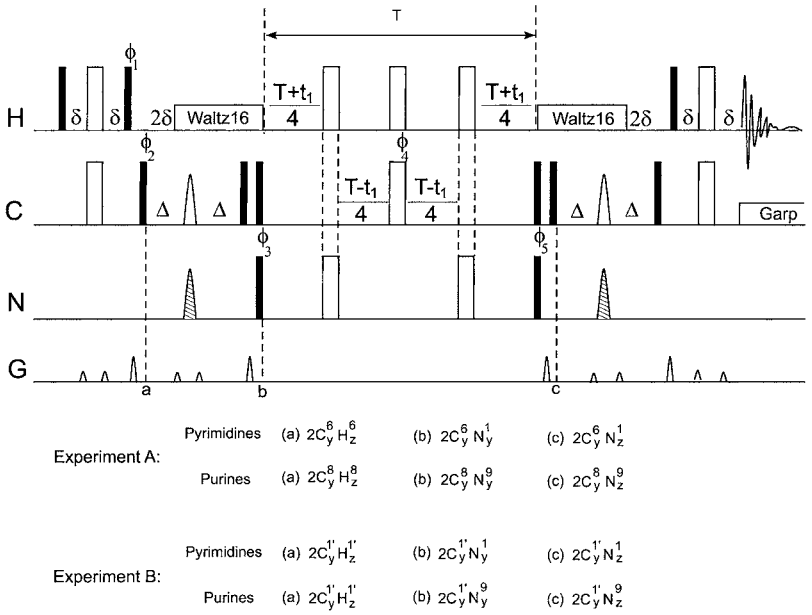

Figure 2. Pulse scheme for measuring CSA/DD cross-correlated relaxation rates $\Gamma_{N,CH} + \Gamma_{C,NH}$ of HCN spin systems in nucleic acids. Filled and open rectangles represent non-selective 90° and 180° pulses. The shaded pulses on ^{15}N represent band selective 180° pulses for Experiment A and non-selective 180° pulses for Experiment B. The two outer 180° ^{1}H pulses in the interval T were 90_x-180_y-90_x composite pulses. For Experiment A, the delays were $\delta = 1.25$ ms, $2\Delta = 21$ ms and $T = 2/J(C5C6) = 30$ ms. Band selective pulses were 1.93 ms REBURP on ^{13}C centered at 137 ppm covering the chemical shift range of C8 and C6 carbons and 1.86 ms IBURP-2 on ^{15}N centered at 159 ppm covering the chemical shift range of N1 and N9 nitrogens. For Experiment B, the delays were $\delta = 1.49$ ms, $2\Delta = 22$ ms and $T = 1/J(C1'C2') = 25$ ms. Band selective pulses on ^{13}C were 3.85 ms REBURP centered at 90 ppm covering the chemical shift range of C1′ carbons. The phase cycling was $\phi_1 = 2(y), 2(-y)$; $\phi_2 = (x), (-x)$; $\phi_3 = 4(x), 4(-x)$; $\phi_4 = 16(x), 16(y), 16(-x), 16(-y)$; $\phi_5 = 8(x), 8(-x)$; receiver phase = *abba baab* with $a = (x), (-x), (-x), (x)$ and $b = (-x), (x), (x), (-x)$. Quadrature detection in ω_1 is achieved by States-TPPI of ϕ_3.

k. The spin pair with a dipolar interaction is separated by a distance of r_{jk}. σ_i^{11}, σ_i^{22} and σ_i^{33} are the principal components of the asymmetric CSA tensor. $P_2(\cos\Theta_{nn,jk})$ is the second order Legendre polynomial, with $\Theta_{nn,jk}$ being the angle between the nn component of the CSA tensor and the dipolar interaction jk. The correlation time for isotropic rotation is given by τ_c^{iso}.

In the case of a molecule undergoing anisotropic rotational diffusion, with an axially symmetric diffusion tensor and neglecting internal motions, the expression for the cross-correlation rate becomes more complex (Chung et al., 1992)

$$\Gamma_{i,jk}^{aniso} = \frac{2}{3}\left(\frac{\mu_0\hbar}{4\pi}\right)\frac{\gamma_j\gamma_k}{r_{jk}^3}\gamma_i B_0 \sum_{n=1}^{2}(\sigma_i^{nn} - \sigma_i^{33}) \times \sum_q J(\omega_q), \tag{10}$$

$$J(\omega_q) = \frac{2}{5}\sum_{a=-2}^{2} \mathcal{D}_{a0}^*(\Omega_{nn}^{PD})\mathcal{D}_{a0}(\Omega_{jk}^{PD})\left(\frac{D_a}{D_a^2 + \omega_q^2}\right), \tag{11}$$

$$D_a = 6D_\perp + a^2(D_\parallel - D_\perp), \tag{12}$$

where $D_\parallel$ and $D_\perp$ are the components of the rotational diffusion tensor. The Euler angles Ω^{PD} of the Wigner rotation matrices relate the principal axis frame of the corresponding spin interaction component to the $D_\parallel$ axis of the rotational diffusion tensor. In the case of macromolecules at high fields, high frequency terms of the spectral density are small, hence only terms with $\omega_q = 0$ are significant in Equations 8 and 10. The equations are valid for arbitrary permutations of the CSA axis labels.

In the presence of internal motions, the transformation between the principal axis frames and the diffusion tensor frame is carried out via intermediate coordinate frames corresponding to the axes about which internal motions occur. This allows each degree of motional freedom to be explicitly accounted for. For the case of restricted rotational diffusion about the glycosidic bond (N1-C1′ or N9-C1′), the spectral density function $J(\omega_q)$ in Equation 10 is given by Wittebort and Szabo (1978)

$$J(\omega_q) = \frac{2}{5} \sum_{a,b,b'=-2}^{2} d_{ab}(\beta^{LD}) d_{ab'}(\beta^{LD}) \mathcal{D}^{*}_{b0}(\Omega^{PL}_{nn}) \times \mathcal{D}_{b'0}(\Omega^{PL}_{jk}) \sum_{m=0}^{\infty} A_{bb'm} \left(\frac{D_{am}}{D^2_{am} + \omega^2_q} \right), \quad (13)$$

$$D_{am} = 6D_{\perp} + a^2(D_{\parallel} - D_{\perp}) + D_{int} \left(\frac{m\pi}{2\Delta\chi} \right)^2. \quad (14)$$

The parameters describing the local motion are the rotational diffusion constant for the restricted rotation D_{int} and the angular range of the restricted motion $\Delta\chi$. β^{LD} is the angle between the axis of rotation (glycosidic bond) and the $D_{\parallel}$ axis of the rotational diffusion tensor. The Euler angles Ω^{PL} relates the spin interaction tensor components to the local frame which is defined with the z axis along the glycosidic bond. The series represented by the coefficients $A_{bb'm}$ is rapidly convergent, requiring only about the first ten terms (Wittebort and Szabo, 1978; London and Avitabile, 1978).

Materials and methods

The pulse sequence designed for measuring the cross-correlated relaxation rates involving the CSA of the glycosidic N and CH dipolar interactions is shown in Figure 2. The preparation of the double- and zero-quantum coherences essentially follows the magnetisation transfer schemes employed in HCN correlation experiments in nucleic acids (Sklenar et al., 1993). Following an INEPT transfer from ^{1}H to the directly attached ^{13}C spin, an in-phase transverse ^{13}C component is generated which evolves under the coupling to the glycosidic ^{15}N spin during a period 2Δ. Selective π pulses are applied to C6 or C8 (Experiment A) or C1′ (Experiment B) to suppress the effects of homonuclear scalar carbon-carbon couplings ^{1}J(C1′C2′) or ^{1}J(C6C5) during the interval 2Δ. In Experiment A, selective inversion pulses are also applied to the glycosidic ^{15}N spins to avoid unwanted transfers to other aromatic ^{15}N spins. The relaxation period T is set to n/J(CC) to avoid signal losses arising from the ^{1}J(C5C6) and ^{1}J(C1′C2′) couplings in Experiments A and B respectively. During the relaxation period T, the π pulses are positioned so that only the 'remote' CSA/DD cross-correlations are effective. The relaxation period is followed by two INEPT transfer steps mirroring the initial excitation. In applications to larger nucleic acids, the sensitivity can be improved by applying the TROSY principle during the ^{13}C - ^{15}N magnetisation transfer intervals (2Δ) (Fiala et al., 2000). The advantage would be higher in Experiment A because of the larger CSA's of the aromatic carbons compared to the sugar carbons.

The experiments were performed on a Bruker Avance 600 MHz spectrometer at a temperature of 300 K. Two dimensional spectra were recorded using 256 scans and 60 complex points in the t_1 dimension for Experiment A. In Experiment B, the number of scans was 192, with 50 complex points in the t_1 dimension. The spectral widths were 11 ppm in the ^{1}H dimension and 34 ppm in the ^{15}N dimension. The carrier frequencies were set on the water resonance (4.7 ppm) for ^{1}H and in the center of the N1 and N9 glycosidic nitrogens (159 ppm) for ^{15}N. For Experiment A the carbon carrier frequency was set in the center of the C6 and C8 resonances (137 ppm). In Experiment B the carbon carrier frequency was set in the center of the C1′ resonances (90 ppm). The experiments were carried out on a 2 mM sample of the RNA kissing complex in D_2O containing 100 mM NaCl, 0.1 mM EDTA and 10 mM sodium phosphate buffer at a pH of 6.5.

Results and discussion

The nucleotide sequence of the RNA kissing complex used in this study is shown in Figure 1. The pulse sequence described in the previous section was employed to measure the sum of the 'remote' CSA/DD cross-correlation rates $\Gamma_{N,CH} + \Gamma_{C,NH}$. The spectra obtained by implementing Experiment A and Experiment B are shown in Figures 3 and 4, respectively. The former measures the cross-correlation between the CSA of the glycosidic N and the C8-H8 or C6-H6 dipolar interactions, while the latter measures the cross-correlation between the same glycosidic nitrogen CSA and the C1′-H1′ interaction on the ribose units. In both cases, the ω_1 dimension is labelled by the chemical shift Ω_N of the glycosidic N, while the ω_2 dimension shows the chemical shifts of the protons. The signals are split by the ^{1}J(CH) coupling along ω_1 which are different for ^{1}J(C1′H1′) $\approx$ 168 Hz, ^{1}J(C6H6) $\approx$ 186.5 Hz and ^{1}J(C8H8) $\approx$ 212 Hz. The doublet components have different relaxation rates arising from the CSA/DD cross-correlation. This leads to differential intensities of the components as seen from the one-dimensional sections in Figures 3 and 4.

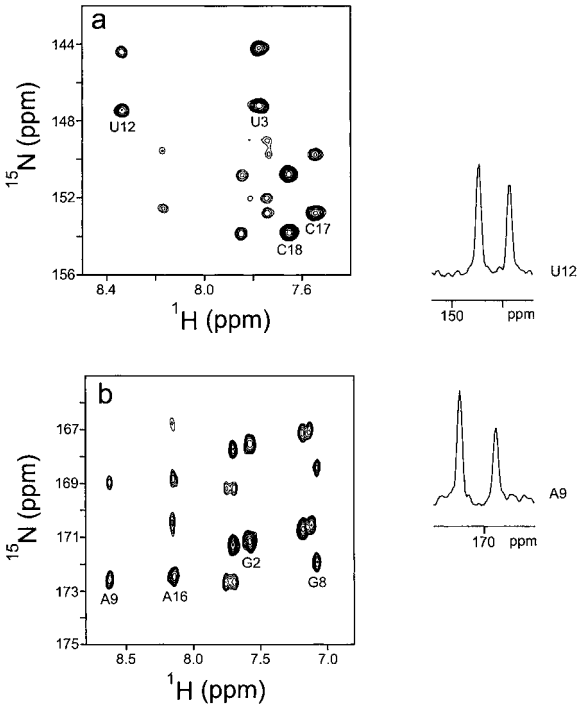

Figure 3. Enlargements of a 2D spectrum obtained by applying the pulse sequence of Figure 2 (Experiment A) to a sample of the RNA kissing complex of Figure 1a. The ^{15}N chemical shift appears along the vertical ω_1 axis and H6 or H8 chemical shifts along the horizontal ω_2 axis. (a) Section showing the resonances from pyrimidine bases. (b) Section showing the resonances from purine bases. Cross-sections along the ω_1 axis show differential line intensities of the doublets arising from CSA/DD cross-correlation effects.

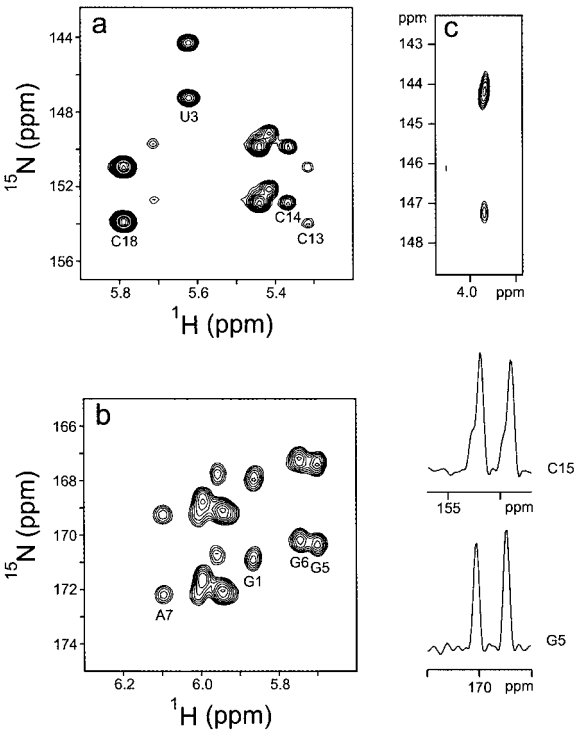

Figure 4. Enlargements of a 2D spectrum obtained by applying the pulse sequence of Figure 2 (Experiment B) to a sample of the RNA kissing complex. The ^{15}N chemical shift appears along the vertical ω_1 axis and H1′ chemical shifts along the horizontal ω_2 axis. (a) Section showing the resonances from ribose units attached to pyrimidine bases. (b) Section showing the resonances from ribose units attached to purine bases. (c) Section from the 2D spectrum showing the U12 residue which has an unusually low chemical shift for the H1′ proton. Some cross-sections along the ω_1 axis are included.

In order to interpret the CSA/DD cross-correlated relaxation rates, some assumptions must be made about the size and orientation of the ^{15}N and ^{13}C CSA tensors in the molecular frame. In a macromolecule like RNA, both the size and orientation of these CSA tensors can vary from one nucleotide to another, even if they belong to same base type, due to differences in local environment. Here we rely on CSA tensor information available from solid state NMR studies and DFT calculations. The CSA tensors of N1 and N9 have been measured experimentally for the nucleic acid bases and the orientation with respect to the molecular framework has been determined with the aid of DFT calculations (Hu et al., 1998). The most shielded (low frequency) component is perpendicular to the plane of the ring while the other two are in the plane of the ring with the least shielded (high frequency) component approximately along the glycosidic N1-C1′ or N9-C1′ bonds. Only in the case of uracil have both orientation and magnitude been determined experimentally (Leppert et al., 2000; Anderson-Altmann et al., 1995). The experimental parameters essentially agree with the conclusions of Hu et al. (1998). The least shielded component subtends an angle $\psi = 15 \pm 5°$ with respect to the N1-C1′ bond and is tilted towards the N1-C2 bond. In our calculations, we have used the magnitudes reported by Hu et al. for the CSA tensors of the four bases (Hu et al., 1998). For the pyrimidine and purine bases we have assumed that $\psi = 18°$ and $0°$, respectively.

If we assume isotropic overall motion of the molecule, the cross-correlation rates would depend largely on the relative orientation of the dipolar interaction with respect to the components of the CSA tensor. Figure 5 shows the angles calculated between the C-H vectors and the principal components of the CSA tensors. The calculations have been carried out for the structure of the kissing complex which has

been determined by NMR (Kim and Tinoco, 2000). It is clear from the figure that the orientations of the C-H vectors of the nucleotide bases do not show major variations with respect to the CSA tensor components for the same base type. In the case of isotropic overall motion one should therefore expect the same CSA/DD cross-correlation rates for all bases of the same type in Experiment A. Also, none of the angles are close to the magic angle (54.74° or 125.26°) and hence relatively large rates can be expected. In the case of ribose units however, the C1′-H1′ vectors have very different orientations with respect to the CSA tensor components even in sugars that are linked to the same base type. Also, most of the angles are close to the magic angle and hence the CSA/DD cross-correlation rates are expected to be much smaller. This is indeed confirmed in Figure 4.

The CSA/DD cross-correlation rates measured in Experiment A are shown in Figure 6. As mentioned previously, the measured rates correspond to a sum of two rates, $\Gamma_{N,CH} + \Gamma_{C,NH}$. The CSA's of aromatic carbons are large and hence the contributions of the term $\Gamma_{C,NH}$ cannot be neglected even if the non-bonded N-H distance is large. In Figure 6a we compare the measured rates with the rates calculated using Equation 8 which assumes isotropic overall motion and negligible internal motions. The calculations have been carried out using a value of $\tau_c^{iso} = 8.9$ ns for the overall motion (Dittmer et al., 2003). Two sets of calculations are presented, one of which considers only the $\Gamma_{N,CH}$ rates while the other includes the contributions of the $\Gamma_{C,NH}$ rates. The non-bonded N-H distance has been calculated for each residue from the NMR structure. To our knowledge, experimental CSA data are not available for the carbons of nucleic acid bases. We have therefore employed the ^{13}C CSA tensors based on DFT calculations reported by Sitkoff and Case (1998) to obtain an estimate of the contribution of $\Gamma_{C,NH}$ to the measured rates. The ^{13}C CSA tensors are fully asymmetric and have their most shielded components perpendicular to the plane of the ring while the least shielded component makes an angle of about 20° with respect to the C-H bond. Comparing the two sets of calculated rates, it is clear that there are significant contributions from the $\Gamma_{C,NH}$ terms. Also there are large differences in the measured rates within each base type, in contrast to expectations for isotropic overall motion.

In Figure 6b, the measured rates are compared with calculations that incorporate anisotropic tumbling with an axially symmetric rotational diffusion

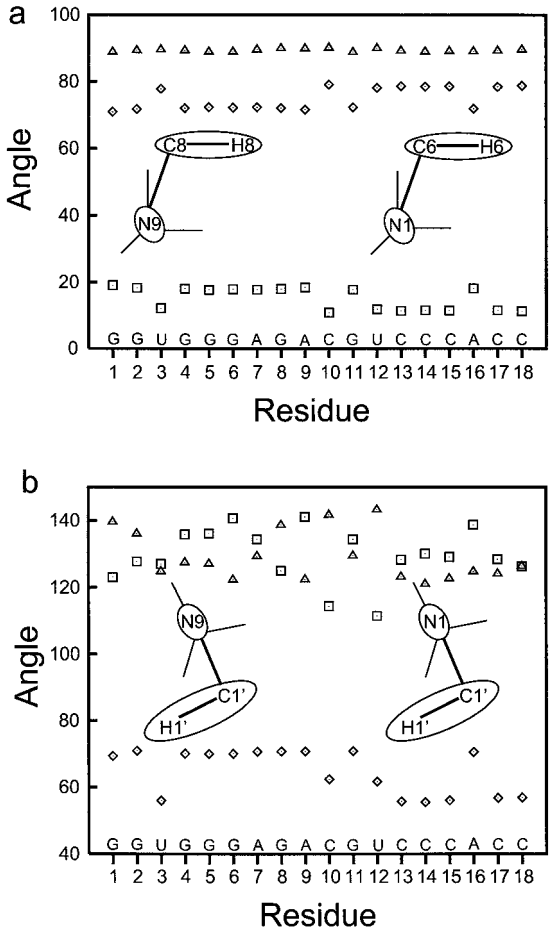

Figure 5. Relative orientations of various magnetic interactions derived from the structure of the RNA kissing complex of Figure 1 determined by NMR (Kim and Tinoco, 2000). (a) Angles between the C6-H6 or C8-H8 dipolar interactions on the aromatic rings with respect to the principal components of the CSA tensors of the N1 or N9 nitrogens in the pyrimidine or purine bases. (b) Angles between the C1′-H1′ dipolar interactions on the ribose units with respect to the principal components of the CSA tensors of the N1 or N9 nitrogens of the corresponding pyrimidine or purine bases. The diamonds denote angles with respect to σ_{11} components (least shielded), squares denote σ_{22} components and triangles denote σ_{33} (most shielded) components.

tensor. The calculations have been carried out using a value of $\tau_c^{iso} = 8.9$ ns and $D_\parallel/D_\perp = 1.9$ (Dittmer et al., 2003) using Equation 10. The parameters τ_c^{iso} and $D_\parallel/D_\perp$ were determined by model-free analysis of the spin-lattice and spin-spin relaxation rates of the imino ^{15}N spins as described by Akke et al. (1997). The correlation time for isotropic motion is related to the average of the rotational diffusion tensor components by $1/6\tau_c^{iso} = D_{iso} = (D_{xx} + D_{yy} + D_{zz})/3$. For axially symmetric rotational diffusion $D_{xx} = D_{yy}$.

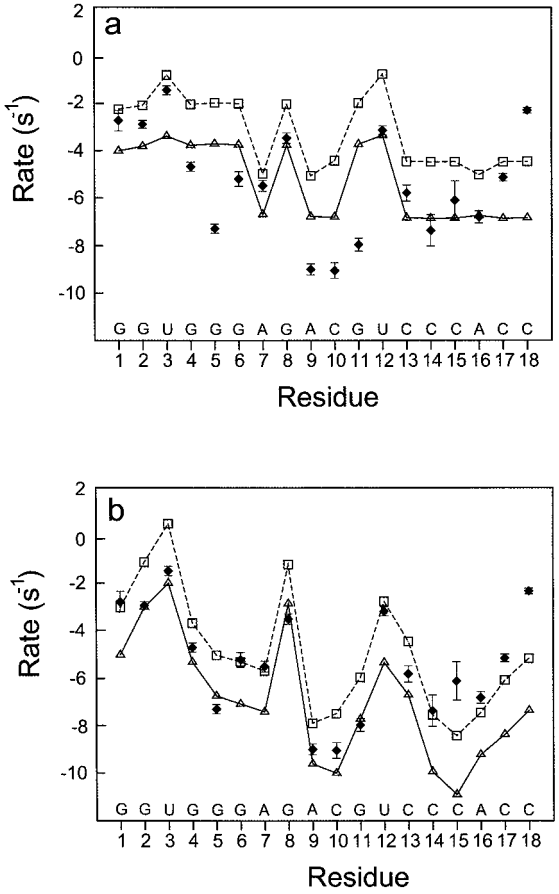

Figure 6. (a) Experimental CSA/DD cross-correlation rates (filled diamonds) due to interactions that are rigidly fixed with respect to each other, measured in Experiment A. Error bars were estimated from the signal-to-noise ratio. The squares connected by dotted lines correspond to calculated $\Gamma_{N,CH}$ rates whereas the triangles connected by solid lines refer to the sum of the calculated rates associated with the short and long range dipolar interactions, $\Gamma_{N,CH} + \Gamma_{C,NH}$, both calculated assuming isotropic overall motion (Equation 8). (b) Same as (a) but with rates calculated assuming anisotropic overall tumbling with an axially symmetric diffusion tensor (Equation 10).

The $D_{\|}$ axis is assumed to be along the length of the complex connecting the C3′ of residue C18 of one unit to the C3′ of residue C18 of the other unit of the dimer. The polar angles which define the orientation of the individual tensor components with respect to the $D_{\|}$ axis were calculated from the NMR structure (Kim and Tinoco, 2000). The calculations show that significant differences in the rates are expected within a given base type, because of the different orientations of the base planes with respect to the $D_{\|}$ axis, even if the spin interactions themselves are rigidly fixed with respect to each other. The measured rates qualitatively agree with the predictions based on anisotropic overall motion. We do not attempt to make a quantitative comparison because of uncertainities in the CSA tensor magnitudes and orientations. However, it might be concluded that the observed rates can probably be accounted for without invoking the presence of internal motions.

In Figure 7 we present the CSA/DD cross-correlation rates measured in Experiment B. The rates have been measured only for those residues that have sufficiently resolved resonances. In this case we do not expect a large contribution from the $\Gamma_{C,NH}$ term because the CSA is expected to be small for the carbons of the ribose unit. The calculated rates assuming either isotropic or anisotropic overall motion do not show a striking difference, in contrast to the cross-correlation rates within the nucleotide base. However, from the rates measured in Experiment A, it is clear that anisotropy of overall motion is significant for this molecule and should be taken into consideration. The interpretation of the CSA/DD rates measured in Experiment B is more complicated because the two spin interactions are located on different structural moeities, namely on the nucleotide base and the ribose unit. The rates are therefore sensitive to the orientation of the ribose ring with respect to the base, to the conformation of the ribose ring and to possible motions about the glycosidic linkage.

On comparing the observed rates with those calculated assuming anisotropic overall motion, the largest deviations occur for the residues G1, G2, C10 and G18. The structural NMR studies have shown that the residues G1, C10 and G18 have sugars that are in a 2′ *endo* conformation or in a mixture of 3′ *endo* and 2′ *endo* conformations suggesting internal dynamics of the sugar ring (Kim and Tinoco, 2000). Recent DFT calculations suggest that the amplitudes and orientations of the ribose ^{13}C CSA tensors have a strong dependence on the ribose sugar puker (Dejaegere and Case, 1998). Calculations of the chemical shift anisotropy for the C1′ carbon in deoxythymidine as a function of the pseudorotation angle have shown that for a typical 3′ *endo* conformation the anisotropy is about 30 ppm whereas for a representative 2′ *endo* conformation it is about 60 ppm. This implies that for sugars in the 2′ *endo* conformation the contribution from the term $\Gamma_{C,NH}$ should be greater than for sugars in 3′ *endo* conformation. At present we do not have a knowledge of the full CSA tensor magnitudes and orientations for the C1′ carbon. Assuming that the C1′ CSA is axially symmetric and using a value of 60 ppm,

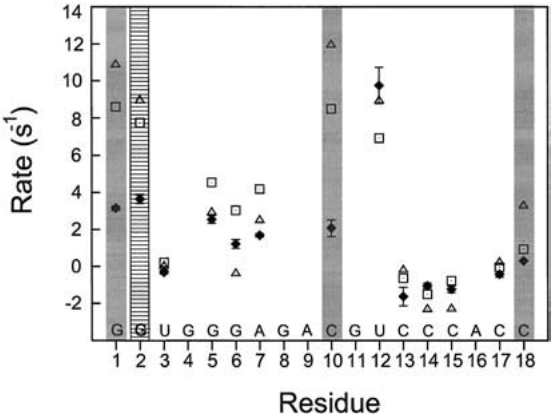

Figure 7. Experimental CSA/DD cross-correlation rates (filled diamonds) due to interactions that are mobile with respect to each other, measured in Experiment B with error bars estimated from the signal-to-noise ratio. The squares correspond to the calculated $\Gamma_{N,CH}$ rates for isotropic tumbling (Equation 8) whereas the triangles refer to rates calculated assuming axially symmetric anisotropic tumbling (Equation 10). Residues which show large deviations between measured and calculated rates even with the model of anisotropic tumbling are emphasised by rectangular strips. Fully shaded strips refer to residues in which strong conformational dynamics of the ribose units are expected (Kim and Tinoco, 2000). No particular dynamics has been reported for the residue G2 (unshaded strip).

we estimate that the contribution of the $\Gamma_{C,NH}$ term could be about -1.0 s^{-1} in the case of isotropic overall motion, leading to a decrease of the sum of the rates $(\Gamma_{N,CH} + \Gamma_{C,NH})$. A more quantitative estimation of the contribution of this term would require a complete knowledge of the CSA tensors.

Previous studies of single quantum relaxation rates of ^{15}N and ^{13}C nuclei in nucleic acids have shown the importance of considering local motions about the glycosidic bonds (Akke et al., 1997; Paquet et al., 1996; Hall and Tang, 1998; Gaudin et al., 1995). The motions of the ribose ring about the glycosidic bond can affect the observed CSA/DD cross-correlation rates. Such motions might be expected to influence the rates measured in Experiment A and Experiment B differently. In the former, there are no relative motions of the CSA and DD interactions, whereas in the latter, the C1′-H1′ orientation with respect to the N CSA tensor can vary. In order to examine the effect of local motions on the rates measured in Experiments A and B, we calculated the CSA/DD rates assuming internal rotations of restricted amplitude about the glycosidic bond. Such motions can result in a diffusional motion of the C1′-H1′ vector about the glycosidic bond between the angles $\chi \pm \Delta\chi$. The spectral density functions for the case of restricted internal rotations occuring in side chains of a macromolecule whose overall motion is described by an axially symmetric diffusion tensor have been derived by Wittebort and Szabo (1978). In the presence of local motions, the spin interactions are no longer rigidly fixed with respect to the diffusion tensor frame. The fluctuations of the spin interactions must be represented with reference to a local frame. The local frame defined with the z-axis along the glycosidic bond rotates with respect to the diffusion frame while the spin interactions are fixed with respect to the local frame. The polar angle β^{LD} between the glycosidic bond and the $D_{\|}$ axis remains fixed, however the azimuthal angle has a time dependence which for the case of restricted rotation results in the spectral density function of Equation (13). The additional parameters which describe the local motions are the rotational diffusion coefficient D_{int} for the internal motion and the angular range of the fluctuation $\Delta\chi$.

In Figure 8 we compare the CSA/DD rates calculated for $\Delta\chi$ values between 40 and 60° with the rates expected for a rigid anisotropic tumbler. The Euler angles Ω^{PL}, relating the CSA tensor components and dipolar interactions to the glycosidic bond, were calculated for each residue from the NMR structure of the complex. The diffusion coefficient for internal rotation about the glycosidic bond was set to a value of $D_{int} = 30 \times 10^7$ s^{-1}. This value was determined by ^{13}C single quantum relaxation rate measurements on a DNA dodecamer (Gaudin et al., 1995). For the range of $\Delta\chi$ values considered, the computed rates were almost insensitive to the internal diffusion coefficient in the range 30×10^6 to 30×10^8 s^{-1}. Only those residues for which internal dynamics of the sugar ring is expected to be large are shown in the figure. In Experiment A, the rates calculated in the presence of local motions lie close to the range of values calculated for the rigid model. On average, the rates calculated in the presence of fluctuations of $\Delta\chi$ between 40 and 60° do not deviate by more than 2.0 ± 1 s^{-1} with respect to the values obtained for the rigid model. In Experiment B on the other hand, the presence of internal motions leads to a significant lowering of the rates. In the presence of $\Delta\chi$ fluctuations, the rates are lowered on average by 10.0 ± 2 s^{-1} with respect to the values obtained from the rigid model. From the calculations we conclude that fluctuations about the glycosidic linkage have a much greater influence on the CSA/DD rates of Experiment B. The four residues which show large deviations of the rates measured in Experiment B with respect to the rigid model calcula-

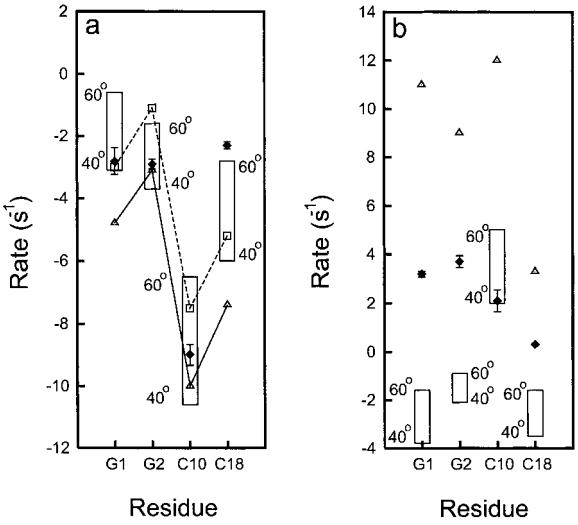

Figure 8. Comparison of CSA/DD cross-correlation rates calculated by considering anisotropic overall motion and rates calculated by including restricted rotations about the glycosidic bond in addition to anisotropic overall motion. Only residues G1, G2, C10 and C18 are shown because they are expected to feature extensive internal motions. The rectangular boxes indicate the range over which the rate varies as the amplitude of the internal rotation about the glycosidic bond changes from 40° to 60°. (a) Calculated rates corresponding to Experiment A, with symbols as in Figure 6. (b) Calculated rates corresponding to Experiment B, with symbols as in Figure 7.

tions are probably subjected to extensive local motions of the ribose unit. Fluctuations about the glycosidic bond do not occur independently but lead to concerted torsion angle fluctuations in the sugar-phosphate backbone and in the sugar ring. Various studies have shown a strong correlation between the glycosidic torsion angle χ (O4-C1′-N1-C2 in pyrimidines and O4-C1′-N9-C4 in purines) and the backbone torsion angle δ (C5′-C4′-C3′-O3), which depends significantly on the sugar pucker (Fratini et al., 1982; Conner et al., 1984; Beckers and Buydens, 1998). It has been suggested that rotations around the glycosidic bond should reflect the fluctuations of sugar puckering (Gaudin et al., 1995). On the basis of the correlations observed between the torsion angles χ and δ, the $\Delta\chi$ range we have considered in the calculations would correspond roughly to a fluctuation of the sugar pucker from the 2′ *endo* region in the pseudorotation cycle to the 3′ *endo* region via the C1′ *exo* conformation (Fratini et al., 1982; Conner et al., 1984).

In the present work, we do not attempt to give a more detailed analysis of the internal dynamics, or to provide a more quantitative estimate of the parameters describing local motions. Except in the simplest cases, where a model of isotropic tumbling is applicable, the analysis of local motions in macromolecules becomes complex because of the large number of motional parameters involved. This becomes further complicated in situations where asymmetric CSA tensors are involved as for ^{13}C and ^{15}N nuclei in nucleic acids. Information on CSA tensors is often only available for small model compounds. A rigorous analysis of relaxation data would require fitting of experimental data to both motional parameters and to the principal axis values and directions of CSA tensors. Such an approach requires the analysis of an extensive set of complementary cross-correlated relaxation rates together with auto-correlated relaxation rates obtained at different magnetic fields. In particular, cross-correlated relaxation rates between the dipolar interaction pairs C1′-H1′/C8-H8 (C6-H6) and C5-H5/C6-H6 can provide complementary information on local motions. The experiments presented in this work offer additional experimental observables that will be useful in more detailed investigations.

Conclusions

Cross correlated relaxation rates involving CSA and dipolar interactions which are either rigidly fixed (Experiment A) or mobile with respect to each other (Experiment B) have been measured in an RNA kissing complex. The measured rates have been analysed in terms of isotropic and anisotropic motional models for the overall motion. For the rigid pair, the influence of the anisotropy of the overall motion is very evident. Measurement of this cross-correlation rate, in addition to the widely used single quantum relaxation rates, would therefore provide additional data to characterize the anisotropy of the overall motion. In order to obtain some insight into the influence of internal motions, calculations based on a model of restricted rotations about the glycosidic bond have been carried out for the cross correlation rates corresponding to Experiments A and B. The calculations indicate that in the presence of internal motions, there is a significant lowering of the rates in Experiment B with respect to the values calculated assuming a rigid model. Among the measured rates, the residues which are expected to have extensive internal motions show the largest deviation with respect to rates calculated for a rigid model. The cross-correlation rates measured in Experiment B therefore help to identify residues with significant local motions.

Acknowledgements

We are indebted to Dr Ignacio Tinoco for his support and encouragement. This work was supported by the Fonds National de la Recherche Scientifique (FNRS) and the Commission pour la Technologie et l'Innovation (CTI) of Switzerland.

References

Akke, M., Fiala, R., Jiang, F., Patel, D. and Palmer, A.G. (1997) *RNA*, **3**, 702–709.

Anderson-Altmann, K.L., Phung, C.G., Mavromustakos, S., Zheng, Z., Facelli, J.C., Poulter, C.D. and Grant, D.M. (1995) *J. Phys. Chem.*, **99**, 10454–10458.

Beckers, M.L.M. and Buydens, L.M.C. (1998) *J. Comput. Chem.*, **19**, 695–715.

Brutscher, B. (2000) *Concepts in Magn. Reson.*, **12**, 207–229.

Brutscher, B., Skrynnikov, N.R., Bremi, T., Brüschweiler, R. and Ernst, R.R. (1997) *J. Magn. Reson.*, **130**, 346–351.

Chiarparin, E., Pelupessy, P., Ghose, R. and Bodenhausen, G. (1999) *J. Am. Chem. Soc.*, **121**, 6876–6883.

Chung, J., Oldfield, E., Thevand, A. and Werbelow, L. (1992) *J. Magn. Reson.*, **100**, 69–81.

Conner, B.N., Yoon, C., Dickerson, J.L. and Dickerson, R.E. (1984) *J. Mol. Biol.*, **174**, 663–695.

Dejaegere, A.P. and Case, D.A. (1998) *J. Phys. Chem. A*, **102**, 5280–5289.

Dittmer, J., Kim, C. H. and Bodenhausen, G. (2003) *J. Biomol. NMR* **26**, 259–275.

Felli, I., Richter, C., Griesinger, C. and Schwalbe, H. (1999) *J. Am. Chem. Soc.*, **121**, 1956–1957.

Fiala, R., Czernek, J. and Sklenar, V. (2000) *J. Biomol. NMR.*, **16**, 291–302.

Fratini, A.V., Kopka, M.L., Drew, H.R. and Dickerson, R.E. (1982) *J. Biol. Chem.*, **257**, 14686–14707.

Gaudin, F., Paquet, F., Chanteloup, L., Beau, J.M., Thuong, N.T. and Lancelot, G. (1995) *J. Biomol. NMR*, **5**, 49–58.

Hall, K.B. and Tang, C. (1998) *Biochemistry*, **37**, 9323–9332.

Hu, J.Z., Facelli, J.C., Aldermann, D.W., Pugmire, R.J. and Grant, D.M. (1998) *J. Am. Chem. Soc.*, **120**, 9863–9869.

Kim, C.H. and Tinoco, I. (2000) *Proc. Natl. Acad. Sci.*, **97**, 9396–9401.

Kumar, A., Grace, R.C.R. and Madhu, P.K. (2000) *Prog. Nucl. Magn. Reson. Spectrosc.*, **37**, 191–319.

Leppert, J., Heise, B. and Ramachandran, R. (2000) *J. Magn. Reson.*, **145**, 307–314.

Lipari, G. and Szabo, A. (1982) *J. Am. Chem. Soc.*, **104**, 4546–4559.

London, R.E. and Avitabile, J. (1978) *J. Am. Chem. Soc.*, **100**, 7159–7165.

Palmer, A.G. (1997) *Curr. Opin. Struct. Biol.*, **7**, 732–737.

Palmer, A.G., Williams, J. and McDermott, A. (1996) *J. Phys. Chem.*, **100**, 13293–13310.

Paquet, F., Gaudin, F. and Lancelot, G. (1996) *J. Biomol. NMR.*, **8**, 252–260.

Reif, B., Hennig, M. and Griesinger, C. (1997) *Science*, **276**, 1230–1233.

Richter, C., Reif, B., Griesinger, C. and Schwalbe, H. (2000) *J. Am. Chem. Soc.*, **122**, 12728–12731.

Schwalbe, H., Carlomagno, T., Hennig, M., Junker, J., Reif, B., Richter, C. and Griesinger, C. (2001) *Meth. Enzymol.*, **338**, 35–81.

Sitkoff, D. and Case, D.A. (1998) *Prog. Nucl. Magn. Reson. Spectrosc.*, **32**, 165–190.

Sklenar, V., Peterson, R.D., Rejante, M.R. and Feigon, J. (1993) *J. Biol. NMR*, **3**, 721–727.

Wittebort, R.J. and Szabo, A. (1978) *J. Chem. Phys.*, **69**, 1722–1736.

Yang, D., Gardner, K.H. and Kay, L.E. (1998) *J. Biol. NMR*, **11**, 213–220.

Yang, D., Konrat, R. and Kay, L.E. (1997) *J. Am. Chem. Soc.*, **119**, 11938–11940.